PROCEEDINGS OF SPIE

SPIEDigitalLibrary.org/conference-proceedings-of-spie

Want a PEPSI? Performance status of the recently commissioned high-resolution spectrograph and polarimeter for the 2x8.4m Large Binocular Telescope

Klaus G. Strassmeier, I. Ilyin, M. Weber, A. Järvinen, M. Woche, et al.

Klaus G. Strassmeier, I. Ilyin, M. Weber, A. Järvinen, M. Woche, S. Järvinen, D. Sablowski, M. Mallonn, E. Keles, T. Carroll, M. C. Johnson, C. Bender, R. M. Wagner, C. Veillet, "Want a PEPSI? Performance status of the recently commissioned high-resolution spectrograph and polarimeter for the 2x8.4m Large Binocular Telescope," Proc. SPIE 10702, Ground-based and Airborne Instrumentation for Astronomy VII, 1070212 (6 July 2018); doi: 10.1117/12.2311627

SPIE.

Event: SPIE Astronomical Telescopes + Instrumentation, 2018, Austin, Texas, United States

Downloaded From: https://www.spiedigitallibrary.org/conference-proceedings-of-spie on 06 Dec 2019 Terms of Use: https://www.spiedigitallibrary.org/terms-of-use

Want a PEPSI? Performance status of the recently commissioned high-resolution spectrograph and polarimeter for the 2x8.4m Large Binocular Telescope

Klaus G. Strassmeier*[a], I. Ilyin[a], M. Weber[a], A. Järvinen[a], M. Woche[a], S. Järvinen[a], D. Sablowski[a], M. Mallonn[a], E. Keles[a], T. Carroll[a], M. C. Johnson[b], C. Bender[c], R. M. Wagner[d], C. Veillet[d]
[a]Leibniz-Institute for Astrophysics (AIP), An der Sternwarte 16, D-14482 Potsdam, Germany;
[b]Department of Astronomy, Ohio State University, Columbus, OH 43210, USA;
[c]Steward Observatory, University of Arizona, Tucson, AZ 85546, USA;
[d]Large Binocular Telescope Observatory (LBTO), Tucson, AZ 85546, USA.

ABSTRACT

PEPSI is the new fiber-fed and stabilized "Potsdam Echelle Polarimetric and Spectroscopic Instrument" for the Large Binocular Telescope (LBT). It covers the entire optical wavelength range from 384 to 913 nm in three exposures at resolutions of either $R=\lambda/\Delta\lambda$=50,000, 130,000 or 250,000. The R=130,000 mode can also be used with two dual-beam Stokes IQUV polarimeters. The 50,000-mode with its 12-pix sampling per resolution element is our "bad seeing" or "faint-object" mode. A robotic solar-disk-integration (SDI) telescope feeds solar light to PEPSI during day time and a 450-m fiber feed from the 1.8m VATT can be used when the LBT is busy otherwise. CCD characterization and a removal procedure for the spatial fixed-pattern noise were the main tasks left from the commissioning phase. Several SDI spectral time series with up to 300 individual spectra per day recovered the well-known solar 5-minute oscillation at a peak of 3 mHz (5.5min) with a disk-integrated radial-velocity amplitude of only 47 cm/s. Spectral atlases for 50 bright benchmark stars including the Sun were recently released to the scientific community, among them the ancient planet-system host Kepler-444. These data combine PEPSI's high spectral resolution of R=250,000 with signal-to-noise ratio (S/N) of many hundreds to even thousands covering the entire optical to near-infrared wavelength range from 384 to 913 nm. Other early science cases were exoplanet transits including TRAPPIST-1, a spectrum of Boyajian's star that revealed strong and structured but stable ISM Na D lines, a spectrum of ζ Oph allowing a redetermination of the ISM Li line doublet, and a first Doppler image of the young solar analog EK Dra that revealed starspots with solar-like penumbrae.

Keywords: instruments, spectrographs, spectropolarimetry, spectral atlases, solar spectra, LBT, PEPSI

1. INTRODUCTION

High-resolution spectra can confine most astrophysical parameters once the data reach a quality appropriate for the various physical processes that form these spectra. Solar spectrum atlases with unprecedented resolution and S/N are the best examples for the power of high-resolution spectroscopy. Intrinsic line-profile variability became the limit for precision, in particular for the Sun but also for stars due to p-mode oscillations and rotationally modulated magnetic activity. Besides intrinsic variability, one extra source of uncertainty is the blending due to finite spectral resolution.

The data in the *Gaia* benchmark spectral library collected by Blanco-Cuaresma et al. (2014) [2] represent the state-of-the-art of high-resolution optical spectroscopic data and correspond in practice to $R=\lambda/\Delta\lambda \approx$70,000 and S/N of several hundred. The vast majority of these spectra are from HARPS (Mayor et al. 2003 [3]) with an original resolution of 115,000. NARVAL (Auriere 2003 [4]) and ESPaDOnS spectra have an average resolution of 65,000 (Paletou et al. 2015 [5]), and the UVES data (Dekker et al. 2000 [6]) have 78,000–115,000. Peak S/N of 150 to 820 are achieved. Higher S/N was obtained for bright stars in the UVES-POP library (Bagnulo et al. 2003 [7]) but with the lower spectral resolution of ≈80,000. Yet, if some of the most decisive astrophysical processes are to be detected and characterized in spectra, it requires much higher spectral resolution and even higher S/N, and thus even larger telescopes (c/o Fig. 1, see also Dravins 2010 [8]).

*kstrassmeier@aip.de; phone +49 331 7499-223; https://pepsi.aip.de/

Ground-based and Airborne Instrumentation for Astronomy VII, edited by Christopher J. Evans, Luc Simard, Hideki Takami,
Proc. of SPIE Vol. 10702, 1070212 · © 2018 SPIE · CCC code: 0277-786X/18/$18 · doi: 10.1117/12.2311627

Downloaded From: https://www.spiedigitallibrary.org/conference-proceedings-of-spie on 06 Dec 2019
Terms of Use: https://www.spiedigitallibrary.org/terms-of-use

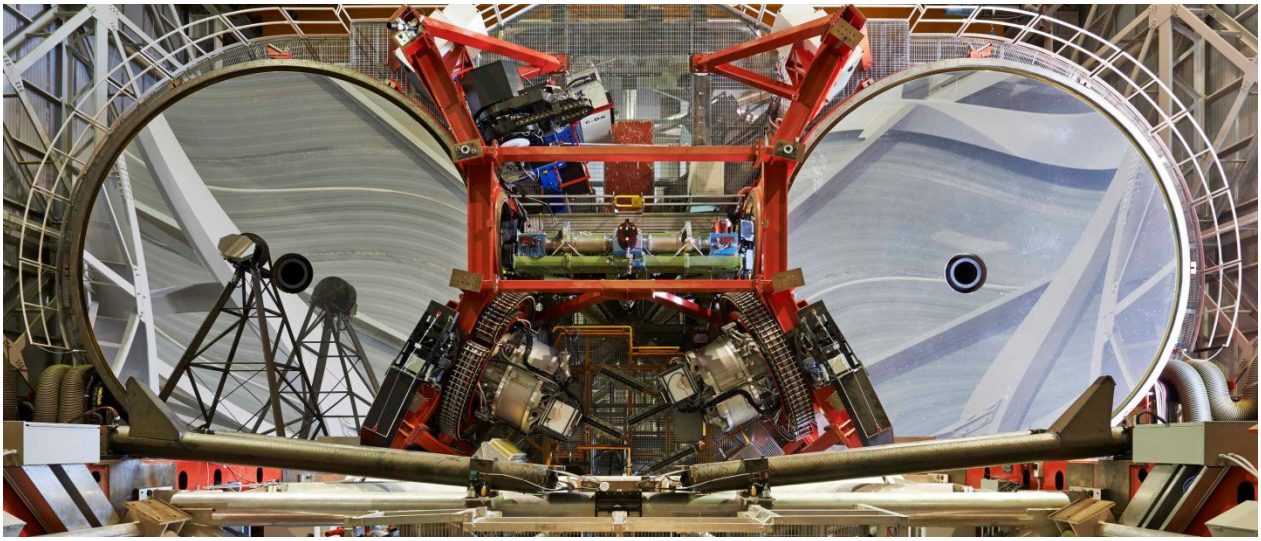

Figure 1. High-resolution spectroscopy requires a large telescope in case high S/N is desired (always is!). PEPSI's home is the currently largest telescope in the world on a single mount, the Large Binocular Telescope (LBT). The picture shows the two 8.4m mirrors in a face-on position. The two PEPSI permanent fiber units are the two tilted white boxes near the upper rim of the picture. Credit: LBTO.

2. BRIEF DESCRIPTION OF THE INSTRUMENT

New values in this paper replace the numbers in the initial technical description in Strassmeier et al. (2015) [1].

2.1 Spectrograph

PEPSI is an asymmetric white-pupil echelle spectrograph in Littrow configuration with an echelle grating with a blaze angle, θ, of 75.27° (R4) and a collimated beam diameter, d, of 200mm which convert to the standard resolution times slit product of $R\alpha = 2d \tan \theta/D$ = 34,600, where D is the telescope diameter of a single LBT eye (D = 8.4m). Figure 2 are pictures of the spectrograph. The optical design is based on a dual arm white-pupil configuration where the main collimator and the two transfer collimators are off-axis Maksutov systems, reaching a near diffraction limited optical quality over a large field of view. This enables relatively long slits as required for recording four sliced spectra simultaneously (two per telescope). At the field lens, located at the intermediate focal plane between the main- and the transfer-collimators, the light is diverted into the blue and the red arms by either one of two selectable dichroic lenses. The off-axis Maksutov transfer systems include a beam diameter reduction from 200mm to 125mm in the blue-transfer and the red-transfer collimators. A set of three VPH grisms for cross dispersion are available per arm. The two f/3 spectrograph cameras are each equipped with a monolithic 10.3k×10.3k Semiconductor Technology Associates (STA) 1600LN CCD with 9 μm pixels.

2.2 User modes

Figure 3 summarizes the user modes. PEPSI can be used with three telescopes, either the 2×8.4m LBT, the 1.8m Vatican Advanced Technology Telescope (VATT), or the 1cm Solar-Disk-Integrated (SDI) telescope. Fiber lengths are 44m, 450m, and 50m for the three telescopes, respectively. While the VATT and the SDI provide integral light only, the LBT also enables polarized light. This makes four fundamental user modes as shown in Fig. 3. The LBT provides regular spectroscopy through a permanent focal station in the bent Gregorian foci. Three spectral resolutions can be chosen by selecting different fibers with different image slicers; R=50,000 (through a 2.3" aperture on the sky sampled by 12 pixels on the CCD), R=130,000 (1.5" aperture with a 4.2-pix sampling), or R=250,000 (0.74" aperture, 2.0-pix sampling).

Downloaded From: https://www.spiedigitallibrary.org/conference-proceedings-of-spie on 06 Dec 2019
Terms of Use: https://www.spiedigitallibrary.org/terms-of-use

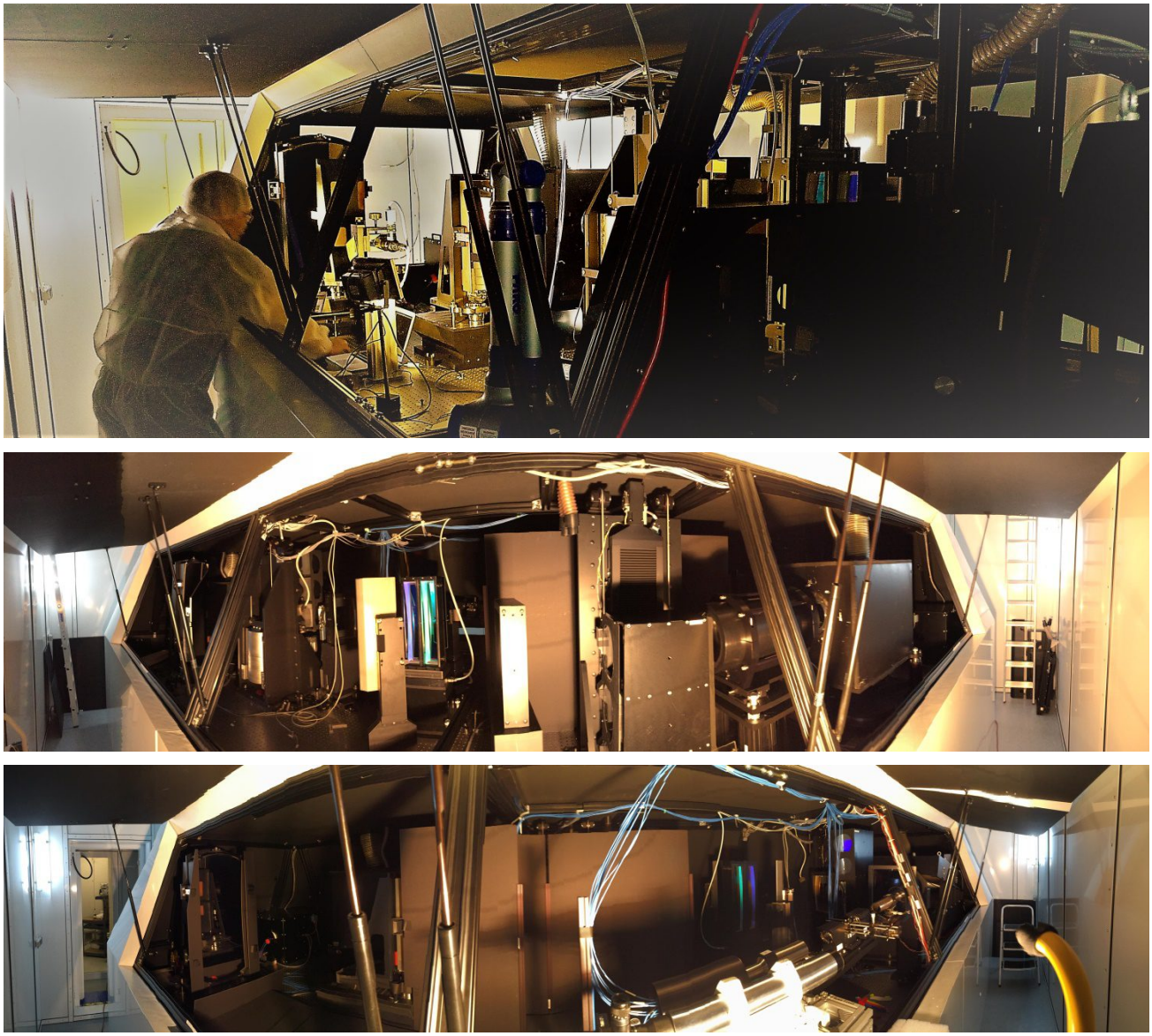

Figure 2. Open hatches of the inner cover around the spectrograph. The table dimensions are 6×2m. *Top:* On the left edge is the main collimator mirror seen, the blue-arm transfer collimator mirror is just close-by to the right. The grating is in the black box to the very right of the picture. *Middle:* panoramic view of the red-arm side. *Bottom:* panoramic view of the blue side-arm side.

Full wavelength coverage is possible with three exposures for all resolution modes. A single exposure always employs two cross dispersers (CD) simultaneously, one in each of the two spectrograph arms. The two cross dispersers in the "blue" and the "red" arm of PEPSI that are adjacent in wavelength, i.e. CD-III and CD-IV, cannot be used simultaneously because of the dichroic beam splitter. All other combinations are possible. Because PEPSI has two beam splitters that are selected automatically depending upon the CD selection, no wavelength gaps exist. The user may also specify that the sky fibers provide fringes from a Fabry-Perot Etalon (FPE) instead of sky background light. This is what we call the high-precision RV mode. The simultaneous FPE spectrum is automatically chopped into sub-exposures of total duration equaling that of the science exposure and need not be specified by the user. This ensures proper exposure time for the fringes and comparable photo centers between science and calibration spectrum.

Downloaded From: https://www.spiedigitallibrary.org/conference-proceedings-of-spie on 06 Dec 2019
Terms of Use: https://www.spiedigitallibrary.org/terms-of-use

Spectropolarimtery is not permanently available. If polarized light is desired, then the two polarimeters must be mounted. In polarization mode the target and the sky fibers are used for the celestial target's ordinary- and extra-ordinary beam. The two PEPSI polarimeters each provide the full Stokes IQUV vector and are modular in design but spectroscopy is only possible with a single resolution, i.e., R = 130,000. Two science modes are currently implemented, firstly, all Stokes parameters consecutively with both telescopes simultaneously (SX and DX give a combined 11.8m aperture) and, secondly, circular Stokes V polarization on SX and linear Stokes QU on DX simultaneously (each with an 8.4m aperture). It takes two spectra for Stokes V and four spectra for Stokes Q and U. Retarder angles are 45° and 135° for Stokes V, position angles of the Foster prism are 0° and 90° for Q and 45° and 135° for U.

SDI spectra are possible with only the ultra-high resolution R=250,000. We run two observing modes with SDI. The default is a daily "deep" spectrum for the full wavelength range at maximum possible S/N. This translates to taking 100 single exposures in each of the three combinations of CD pairs. Exposure time varies strongly with wavelength (15s in the very blue to 1.5s in the very red) and typically allows for three consecutive such deep spectra per day. The other mode with SDI is a time series mode. The user simply selects a pair of CDs and the robot takes spectra from dawn to dusk. This mode allows up to 1,000 individual spectra per day with a cadence of 92 s (see Strassmeier et al. 2018a [9]). Note that we are currently in the middle of an attempt to shorten the cadence by optimizing the communication time between the CCD controller and the local-area network.

The light feed from the 1.8m VATT was originally implemented for commissioning but is now available for 50 nights per year for science. It provides a spectral resolution of R=200,000 with a large 3" aperture on the sky and a 200-µm fiber. No sky fiber is provided with the VATT but a second image slicer is available and can be fed simultaneously with FPE fringes. Due to the long fiber connection of 450m, the VATT is mostly recommended for the red arm of PEPSI because of the strong attenuation of blue light in the fiber.

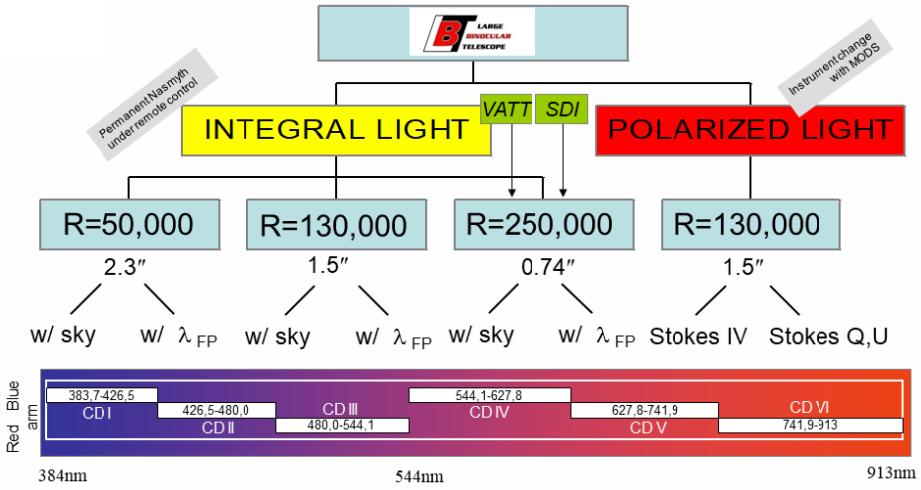

Figure 3. PEPSI user modes. Three telescopes can feed PEPSI (LBT, VATT, and SDI). If on the LBT, one can choose between integral and polarized light. Numbers in the graph below the spectral resolutions R are the fiber-core diameters projected on the sky in arc sec. The colored bar indicates the spectrograph with its six cross dispersers (number I to VI from left to right). Listed are their wavelength coverages in nm. Two cross dispersers are always used simultaneously for one exposure.

2.3 Wavelength coverage

The possible wavelength coverage is from 3825-9135 Å. The very edges of the spectrum are not really useful because the respective orders only partially fit on the CCD and appear asymmetrically truncated. Tracing a part of them is possible but strongly depends on the S/N there. For bright stars, we have added the two partial orders at the two wavelength ends and then gained the above cited full coverage. Otherwise, we extract only the full orders and then end up with a nominal wavelength coverage of 3835-9065 Å.

Downloaded From: https://www.spiedigitallibrary.org/conference-proceedings-of-spie on 06 Dec 2019
Terms of Use: https://www.spiedigitallibrary.org/terms-of-use

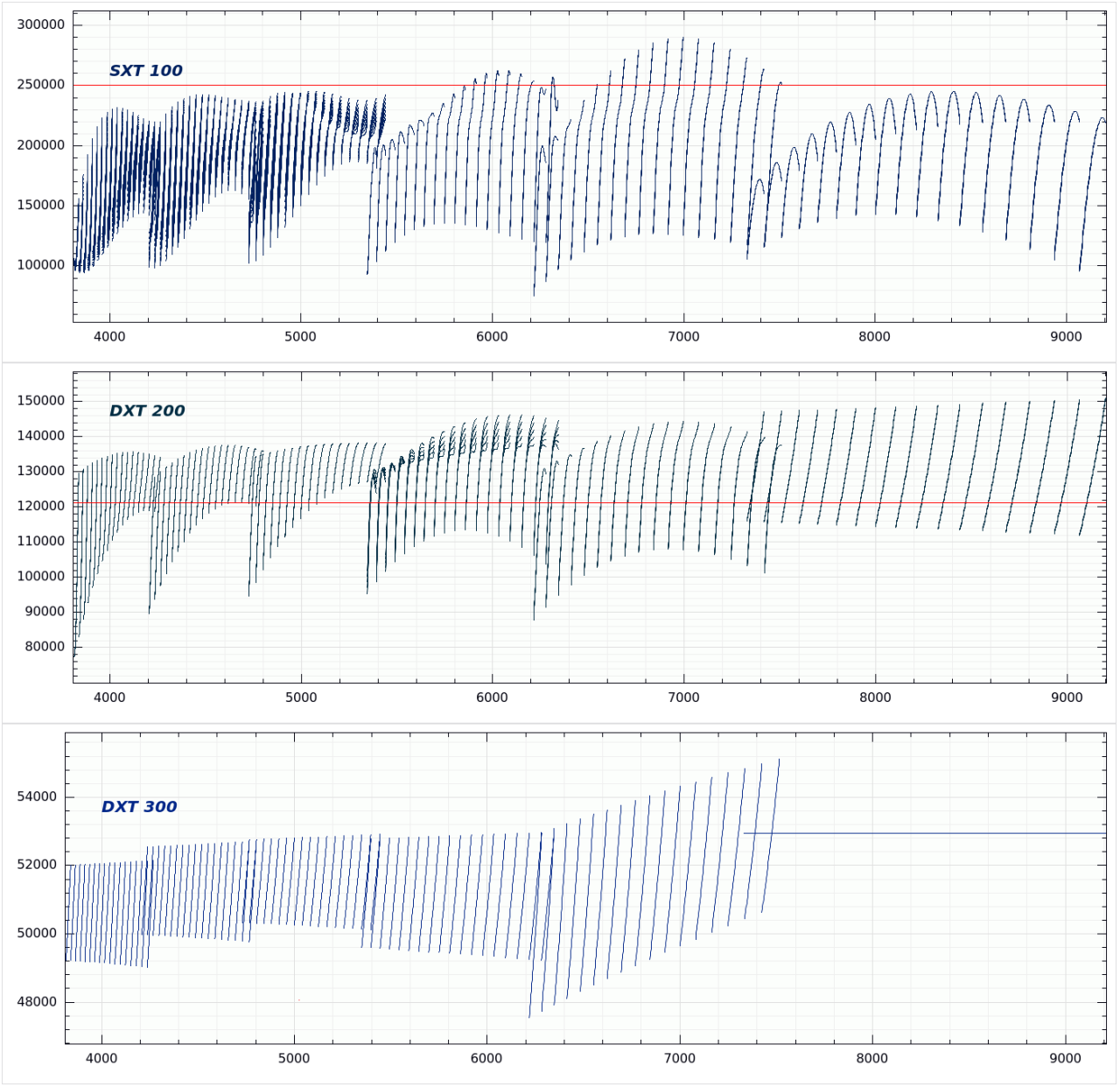

Figure 4. Spectral-resolution plots for Feb. 2018. Only the DX telescope is shown. The panels plot $R=\lambda/\Delta\lambda$ vs. wavelength in Ångströms for the fiber core diameters of, from top to bottom, 100µm and 7-slice image slicer, 200µm and 5-slice slicer, and 300µm and 3-slice slicer, respectively. The horizontal red lines in the top two panels indicate the expected resolution. For the 300µm fiber in the lower panel, only the average of all slices is shown. See text.

2.4 Spectral resolution

PEPSI achieves its spectral resolution by using stacks of waveguide image slicers with 3, 5, and 7 slices per slicer coupled to 300µm, 200µm, and 100µm core-diameter fibers, respectively. The actual spectral resolution in the ultra-high resolution mode (100µm fiber) strongly depends on the achieved focus across the 10k CCD. Focus position is adjustable by moving the two optical cameras with respect to the CCD. While for the 200µm and 300µm fibers this is not an issue,

Downloaded From: https://www.spiedigitallibrary.org/conference-proceedings-of-spie on 06 Dec 2019
Terms of Use: https://www.spiedigitallibrary.org/terms-of-use

image quality across the two diagonals of 140mm of the CCD is the limiting factor for the resolution in the 100µm fiber mode. Figure 4 shows example resolution plots for the same and fixed focus for each blue and red cross disperser, respectively, and for every echelle order and each slice (except for the 3-slice slicer). Note that the expected resolution for the 300µm mode is 43,000 but actually 48-54,000 is achieved due to better image-slicer geometry than designed.

2.5 Efficiency

This is still work in progress. A very recent measurement with a HeNe laser of the 200µm fiber mode gave a peak efficiency of 6.2% at 700 nm including the telescope. Given that the photon sees 65 optical surfaces until it arrives on the CCD, this is a reasonable value but currently below expectation. So far we could not identify a particular optical component that is grossly out of specification but mostly a slightly lower than predicted performance of nearly all components. One suspicion was enhanced guiding jitter under not perfect seeing conditions. A recent realignment of the DX PFU with respect to the telescope resulted in new guider offsets as well as a better pupil position on the two (Shack-Hartmann) wave-front sensors. It removed the earlier jitter issue and a test run with guiding for 30 min under good but not perfect seeing conditions (average 0.9″) showed a guiding rms of only 0.17″ on SX and 0.12″ on DX. This captures close to 100% of the flux even for the 200µm fiber mode (1.3″ aperture) and still about 80-90% for the 100µm fiber mode (0.74″ aperture) and all of it for the 300µm fiber (2.3″ aperture).

2.6 Polarimeters

The two polarimeters are basically identical. Both are based on a classical dual-beam design with a modified Foster prism with two orthogonally polarized beams in parallel. The Foster prism along with its ADCs, one per beam, and the reimaging cameras and fiber heads are rotatable with respect to the sky. The retarder in front of the Foster can be inserted when circular polarization (CP) is measured and be removed from the beam when linear polarization (LP) is measured. This has the big advantage of no cross talk between CP and LP. Standard-star tests included a so-called null spectrum, which is obtained by swapping the observation sequence in the two beams. Ideally, it would give zero polarization and be independent of wavelength. Any residual polarization would be due to instrumental effects. The null spectrum for PEPSI shows an extraordinary low degree of polarization noise for an exposure on the bright magnetic star γ Equ, better by a factor of 2.5 with respect to a two-times longer integration with the HARPS polarimeter (Fig. 5).

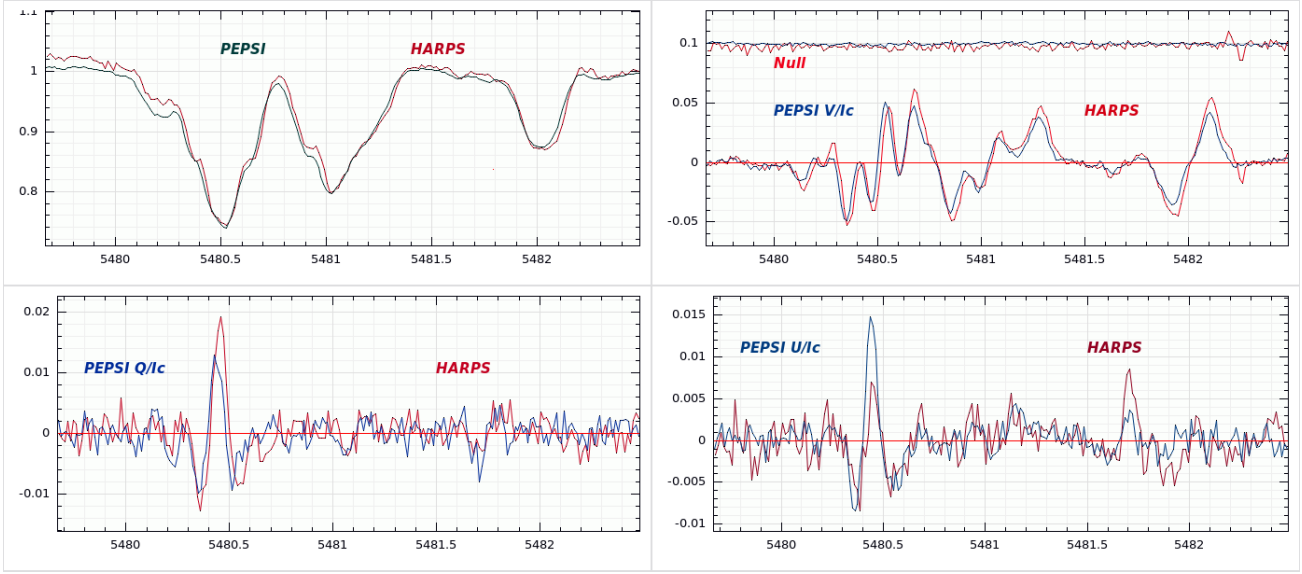

Figure 5. First polarimetric spectrum from PEPSI. The target is the bright magnetic A9VpSrCrEu star γ Equ. The blue line is the PEPSI spectrum and the red line is, for comparison, a HARPS-Pol spectrum. From top left to bottom right: the normalized integral light I/Ic; the normalized circular component V/Ic and, in the top, the magnetic null spectrum, both enlarged by a factor five; the normalized linear component Q/Ic enlarged by a factor 5; and the normalized linear component U/Ic also enlarged by a factor 5. S/N of the PEPSI spectrum is 1180, that of the HARPS spectrum 450. The *x*-axis is wavelength in Ångströms. More details in Sect. 6.5.

Downloaded From: https://www.spiedigitallibrary.org/conference-proceedings-of-spie on 06 Dec 2019
Terms of Use: https://www.spiedigitallibrary.org/terms-of-use

3. RECENT HARDWARE REPLACEMENTS AND UPGRADES

3.1 Coatings

The blue-arm optics were dismantled over winter 2015/16 and sent to two different companies for recoating. All coatings were out of spec at the blue wavelength edges. The (blue) transfer collimator mirror had first to be sent to the producer in France for removing the old silver coating because it required re-polishing of the carrier. The transmission optics and the re-polished reflective optics were re-coated at Quantum Optics with a superior UV-enhanced silver coating and were reintegrated on the mountain in March 2016. A new set of slightly larger folding mirrors with the same silver coating was also implemented.

3.2 Image slicers and fiber injection

PEPSI employs a total of 20 fixed image slicers blocked together on a single Zerodur carrier. Each fiber from the telescope has its own slicer. The slicers themselves are of a waveguide type with stacks of plane-parallel glass plates of different thickness and numbers depending on how often the fiber exit is to be sliced. The regular R=250,000-mode is provided with a 7-slice stack in combination with 100µm fibers, the 130,000-mode with a 5-slice stack and 200µm fibers, and the 50,000-mode with a 3-slice stack and 300µm fibers. The slicers and their production were described in detail in Beckert et al. (2016 [10]). In 2016, we replaced the original image slicer prototype with the final version shown in Fig. 6. The slicer geometry was optimized compared to the previous version, as was the manufacturing process at IOF in Jena. More care was taken to block stray light at both entrance and exit sides. For example, an aperture mask was placed around the illuminated slices by (optically) gluing it onto the slicer entrance and exit surfaces. The mask is made of quartz and is also AR coated on its air surface, minimizing losses at the respective slicer entrance and exit surfaces. The original slicer injection optics, which consisted of three mirrors (two off-axis, one plane) to transfer the fiber exit f/3 to the collimator f/13.9, was very hard to align with the accuracy needed to uniformly illuminate the slices, which led to degraded image quality for the ultra-high resolution mode. We therefore replaced it by a lens-based system. It was designed for a bigger field-of-view than the old one in order to allow for two additional slicer modes specifically designed for the fiber feed from the SDI telescope and the VATT. Because the main slicer modes are made for the two telescopes of the LBT, the space needed on the detector for the VATT could be more efficiently used with an extra ultra-high resolution mode called 100L (9 slices with each slice of 70µm width; R=260,000) without an efficiency penalty. The regular VATT mode with the 130L slicer-fiber combination remains at R=200,000 (9 slices each 100µm width). The SDI telescope still consists of two fibers and is equivalent to the 100L mode of the VATT. Figure 7 shows a cut along a CCD column for one echelle order for the 100µm modes for the LBT and the VATT.

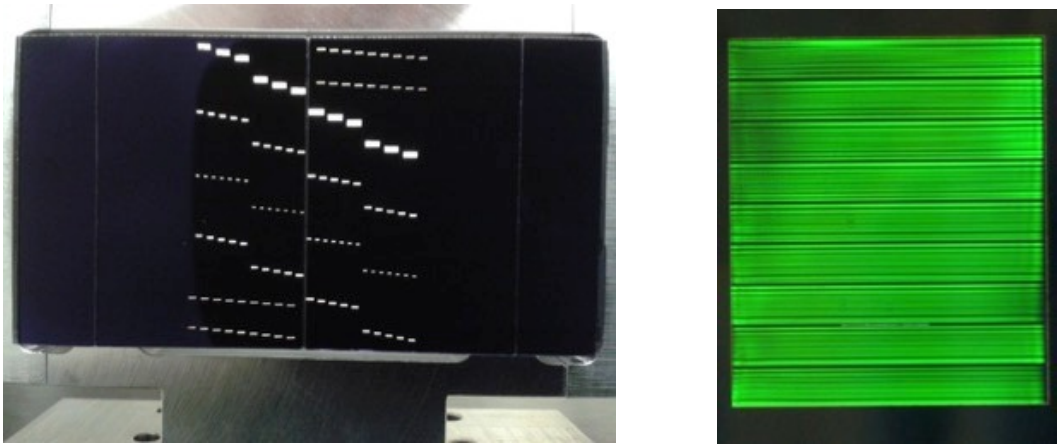

Figure 6: *Left:* Front view (exit side) of the new PEPSI image slicer. On the bottom of the left half side (for SX) and the top of the right half side (for DX) one can see the four new 9-slice slicers for the SDI telescope and the VATT, which are designed for use with a single target and a single calibration spectrum. It provides R=200,000 at the VATT (130L mode) and also allows for R=260,000 but using a larger 200µm fiber instead of the 100µm on the LBT (100L mode). *Right:* Entrance side of one of the new image slicers; here DX-100L. Its 9 slices, each 70µm thick, spread the light over a larger area on the CCD than before.

Downloaded From: https://www.spiedigitallibrary.org/conference-proceedings-of-spie on 06 Dec 2019
Terms of Use: https://www.spiedigitallibrary.org/terms-of-use

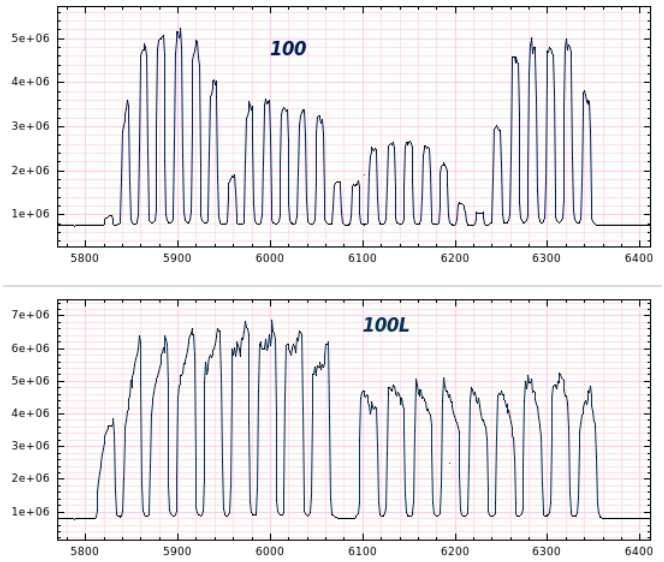

Figure 7. CCD cross-cut through one échelle order for the ultra-high resolution modes on the LBT and the VATT (dubbed "100" for the corresponding fiber-core diameter in μm). The *x*-axis shows CCD columns in pixels, the *y*-axis is relative flux. *Top panel:* The four simultaneously recorded spectra at the LBT with 7 slices each (the calibration spectra on the outside, target spectra on the inside). The width of the cross-cut corresponds to the length of the individual slices, while the thickness of the slices makes up one spectral resolution element, which is 70μm corresponding to 2 pixels on the CCD. *Bottom panel:* The same as above but for the two simultaneous spectra when PEPSI is used with the (single-eye) VATT. There, a new 9-slice slicer is employed (left is the target spectrum, right is the simultaneous calibration spectrum).

3.3 CCD systems

Both CCD controllers from ARC were upgraded from their 48C series to the 48D series.

Early on it was noted that the Th-Ar wavelength solution in both Red and Blue CCDs had some kind of discontinuity between the top and the bottom amplifiers as seen in the residuals of the solution. This indicated that some sort of pixel "size" is changing at the very end of each amplifier readout, effectively making the wavelength dispersion at the image center not continuous but having a few-pixel ramp in opposite directions. The timing DPS code had to be adjusted to make the readout of the top and bottom amplifiers to be synchronized with each other. This solved the problem.

One of the 16 amplifiers of the blue 10k CCD had developed reduced quantum efficiency over time. Consequently, the entire dewar was shipped to University of Arizona's Imaging Technology Laboratory (ITL) where loose bonding was found. It altered the impedance such that photoelectrons were lost. At the same time, a severe contamination inside the blue dewar near the pressure sensor was discovered and repaired at the same time. The blue spare CCD controller also had some loose wiring and was also repaired at ITL and brought back to the mountain with the rest of the blue system.

The Red dewar developed a vacuum-leak problem that required frequent pumping a the 1-mbar level. The (identical) Blue dewar remained comparably stable at the same time with an average pressure of 250 μbar. The cause was found to be the outgassing from the optical glue from the CCD window lenses. It required a new design of the flange of that dewar so that the open edges of the optical glue fell now outside of the vacuum volume.

3.4 Chamber

The stabilization of the chamber and its characterization made significant progress but is not final yet. An intermediate cooling water cycle was installed on the PEPSI support bridge that makes the chamber now less prone to the temperature jumps of the LBTO chilled-water supply. Judged from monitoring of the Th-Ar wavelength solutions (every 5 minutes) versus the FPE fringes, we have currently a radial-velocity (RV) stability of 4 m/s rms without taking the FPE drift

Downloaded From: https://www.spiedigitallibrary.org/conference-proceedings-of-spie on 06 Dec 2019
Terms of Use: https://www.spiedigitallibrary.org/terms-of-use

correction into account and for as long as the environmental parameters are not screwed. The latter happened, e.g., for the one instance when one valve of the air-suspended optical table became untight and changed the refractive index of the air inside the chamber. Otherwise, the chamber is stable over months. The rms RV that we got from the solar observations during a series of 8.5 hours of spectra was 1.2 m/s (Strassmeier et al. 2018a [9]). This series was even taken without simultaneous FPE. So the spectrograph can do much better than the 4 m/s rms from Th-Ar, but that is work in progress. The potential can be estimated from our early RV results of a transit of the TRAPPIST-1g planet in Fig. 14.

3.5 Polarimeters

The storage containers in the LBT building were given their environmental supplies (ethernet, glycol) and the assembly tent was converted into a clean environment. A fiber connection within the building was installed so that the polarimeters can be fed by calibration light while still in the storage containers and be connected to the spectrograph. This makes sure that the polarimeters remain always well calibrated and controllable, in particular before they go on the telescope. A complex instrument-lifting tool was designed at AIP and produced at a company in Tucson.

3.6 SDI telescope

Both refracting telescopes were replaced in 2016 with a single reflective telescope feeding an integration sphere. This was inspired in order to be able to obtain also high-precision RVs for the Sun (when observed as a star). Although earlier SDI spectra had shown an excellent wavelength zero point within 10 m/s of the Laser comb wavelengths from the HARPS solar atlas (Molaro et al. 2013 [11]), our RV data appeared with a scatter of up to 100 m/s peak-to-valley. The reason was a too small a field of view of the telescope with respect to the solar disk and caused varying fractions of the disk being seen by the fibers.

4. STA1600LN CCD CHARACTERIZATION

4.1 Gain calibration

The gain relates the number of photoelectrons in a pixel to the number of analog-to-digital units (ADUs) recorded by the CCD camera's software. We have repeatedly measured gain factors for all amplifies on both CCDs and store them in the FITS image where they are available for data reduction. The most recent calibration from 1/2017 gives an average gain for both PEPSI STA1600LN CCDs of around 0.47 e^-/DN.

4.2 Read-out-noise

Read-out-noise (RON) is measured from the bias of the overscan region of each amplifier. It is written into the FITS header of every CCD image that is stored to disk, along with the gain. Both PEPSI CCDs are read out at 125 kHz. We noted a degradation of the RON of the Red CCD system over time. Its average RON appeared to have increased from 4.5 to 8.0 electrons from 2014 to 2018, the cause is still unknown.

4.3 Tool of choice: master flat fields

The master flat field is obtained for each cross-disperser by defocusing the halogen echelle image so that the spectral orders are smeared out on the CCD and partly overlap. A sum of typically 70 individual exposures for each cross disperser is used to make up the master flat-field image. A smoothing spline in clip-and-fit mode is used for every column to remove any gradients due to non-uniform illumination and wavelength dispersion in order to extract the pixel-to-pixel fixed pattern noise of the CCD. Typical S/N achieved is 2,000 per flat-field image and 20,000 for the combined master. Overall pixel-to-pixel sensitivity varies across the blue and red CCDs from 1.5% to 3%, which makes it important to have a proper and accurate correction for the master flat field. The visibility of the remnant CCD wafer structure is most pronounced at red wavelengths and seen as peaks across CCD rows of strength up to 5% at every 165 pixels (Fig. 8). Each such noise peak is split into three sub-peaks separated by 4 pixels. This feature is wavelength dependent and has strongest amplitude in the red. There is also periodic structure in the CCD columns with a period of 330 pixels and noted as a modulation of the fixed pattern noise.

Downloaded From: https://www.spiedigitallibrary.org/conference-proceedings-of-spie on 06 Dec 2019
Terms of Use: https://www.spiedigitallibrary.org/terms-of-use

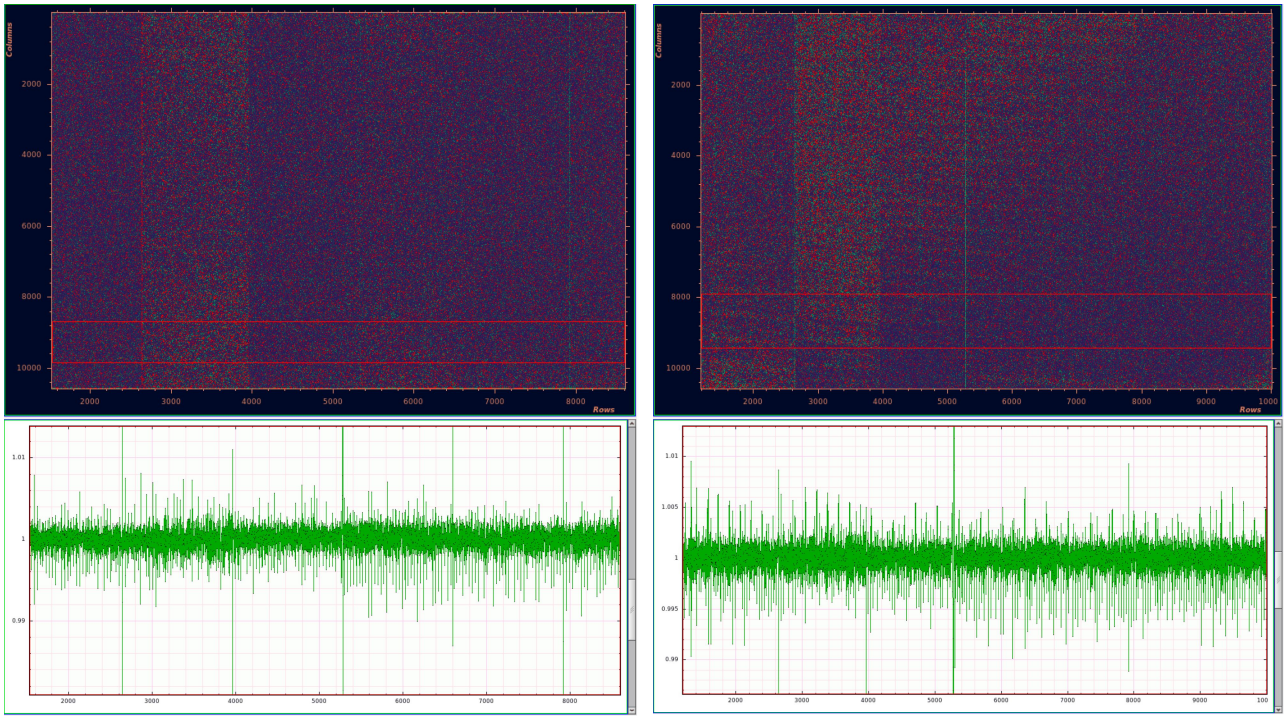

Figure 8: Normalized master flat fields. *Left panels:* for Blue 10k CCD with CD-II (420-480 nm). *Right panels:* for Red 10k CCD with CD-V (630-740 nm). The top panels show CCD rows (*x*-axis) versus columns (*y*-axis). The bottom panels are the averaged cross cuts from the red boxes in the upper panels; *y*-axis is in normalized intensity units with a range of approximately ±1%. The fixed-pattern noise is obvious in form of peaks above and below unity.

4.4 Fixed-pattern noise

Fixed-pattern noise refers to pixel-to-pixel variations with a fixed spatial location on the CCD (see Bredthauer & Boggs 2016 [12] for an update on STA1600LN production). It is typically introduced during the wafer production process, e.g., by the bussing lines each consisting of three electrodes in our case, or remnants from the substrate polishing, and many more. The main problem is that the noise amplitude depends on the illumination (ADU) level and is also wavelength dependent. It affects only certain regions ("taps") on the CCDs, some periodically, some only at a certain pixel. This was and still is the limiting noise source for ultra-high S/N spectra from PEPSI because its removal is not 100% perfect. However, the master flat fields are now being done to a very high precision and already allow science spectra with S/N of 6,000, sufficient even for solar spectra. Previous spectra of some of the bright *Gaia*-benchmark stars from the commissioning period were still limited to S/N approximately 1,500:1 (as stated in Strassmeier et al. 2018b [13]).

A big burden for data reduction is the illumination dependency. The fixed pattern noise amplitude increases non-linearly with exposure time at the 0.1% level when increasing from the default 10 ms to 1,000 ms exposure time. This indicates that there is some sort of reflection from the CCD substrate which increasingly contributes to the fixed pattern noise budget. It requires dimming of the halogen light source for the flat fields and thus takes significantly longer for obtaining the master flat-field image. The final master flat field image is obtained from 2,400 individual flat fields per cross disperser, in total 14,400 exposures. A single master-flat series with 100 exposures takes 2.5 hours. It is repeated with 24 different exposure times (then dubbed a super master flat) and for all six cross dispersers which then takes ≈10 days. Because we may expect additionally a time dependent noise term, we now repeat this exercise from time to time. Notice that the user does not see all these activities because the DR pipeline just prompts for the master flat-field image nearest in time. Figure 9 shows the pixel rms of the condensed fixed-pattern-noise amplitude for a central CCD section as a function of wavelength. It shows that there is basically no wavelength dependency on the Blue 10k CCD for wavelengths of CD-I to CD-III (380-540nm) but strong wavelength dependency on the Red 10k CCD seeing CD-IV to CD-VI (540-910nm), while their respective amplitudes are invers, i.e., larger in the blue and smaller in the red.

Downloaded From: https://www.spiedigitallibrary.org/conference-proceedings-of-spie on 06 Dec 2019
Terms of Use: https://www.spiedigitallibrary.org/terms-of-use

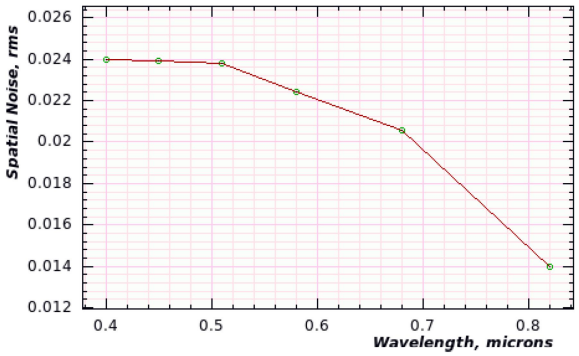

Figure 9. Spatial noise rms in relative units versus central CD wavelength measured in a box of 700×700 pixels at the same central position of the CCDs. The three blue CDs show the highest amplitude but little wavelength dependency whereas the three red CDs show lower amplitudes but a dependency with wavelength.

We have coded a procedure to remove all this illumination- and wavelength-dependent fixed-pattern noise from both 10k CCDs to a best possible level. The result is compared in Fig. 10 for the Red 10k CCD and cross disperser CD-III. The master flat field image in this case was comprised of 100 individual exposures (with bias subtracted). An average of 3,100 columns across all CCD rows with and without fixed-pattern-noise removal is shown in the top panel of Fig. 10. The respective S/N is calculated in a running boxcar window of 33 pixels width for each CCD row and shown in the lower panel. The smooth curved line shows the expected S/N derived from photon statistics. With the spatial noise removed an S/N of up to 20,000 can be achieved and corresponds to the level as expected. Only for two 1,320-pixel row sections ("taps") a less efficient noise reduction is achieved. The red box in the bottom panel corresponds to these two CCD sections. This may possibly indicate that some of the fixed pattern noise in these CCD sections is variable in time.

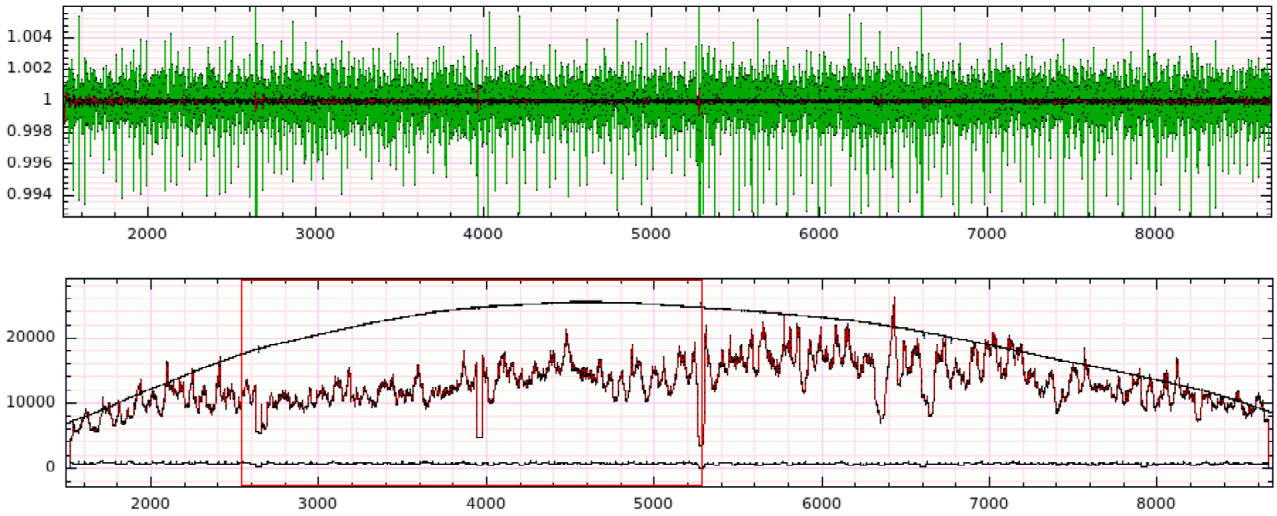

Figure 10. Flat field before and after fixed-pattern-noise removal. *Top panel*: The average of 3,100 CCD columns across rows is shown before correction (green spiky line) and after correction (red straight inner line). *X*-axis is in pixels, y-axis in arbitrary flux units. *Bottom panel:* S/N from the same CCD location as above. The uncorrected flat field (lower nearly straight line) has S/N of just 700 from 3,100 columns. The noise-corrected flat field (rigged line) is close to the expected photon noise (top curved line). In this plot the *x*-axis is in pixels and the *y*-axis is S/N. Two CCD taps with particularly bad behavior are emphasized by the red box. The narrow dips are artifacts due to unaccounted blemishes.

Downloaded From: https://www.spiedigitallibrary.org/conference-proceedings-of-spie on 06 Dec 2019
Terms of Use: https://www.spiedigitallibrary.org/terms-of-use

4.5 Amplifier glowing

Unexpected glow in a single amplifier of both CCDs appeared after replacing the old ARC-48C controller with the new ARC-48D versions in February 2015. The effect was first noticed in April 2015. The old controllers had no noticeable glowing at all. On the Blue CCD the glow rate is 1ADU/min, on the Red it is 2 ADU/min. While the Blue CCD glow location coincides with the position of amplifier #1, the glow location on the Red CCD does not coincides with any amplifier location but appears adjacent to amplifier #16. We have tested for several non-CCD causes, e.g., the pressure sensor in both dewars, the temperature sensor outside the dewar, for parasitic light source, and amplifier voltage settings but did not find a conclusive explanation. So far, the glowing does not affect the spectra.

5. SOFTWARE

5.1 Data reduction

The data-reduction software "SDS4PEPSI" is now complete but not documented yet. At the time of writing, we are also not yet prepared to compare our instrument-related data reduction to the many other existing echelle reduction packages (Reduce, ESpRIT, Echomop, Figaro, ARCES, FEROS, or IRAF/echelle and Midas/echelle). Note that, e.g., IRAF/echelle cannot deal with tilted image slicers. In PEPSI an order is like a tilted Gaussian and it changes across the full wavelength range while the spectral lines are aligned and not tilted. All previously taken PEPSI spectra were re-reduced with what we now call Version 1.0 (see pepsi.aip.de for more details) and thereby optimally extracted, properly stray-light corrected, and continuum normalized. A new data and compute server was required at AIP to run SDS4PEPSI holding now 120 TB and 80 cores.

5.2 Instrument control

Here we just want to re-emphasize that the PEPSI data-reduction software is part of its overall control software (for an overview see Strassmeier et al. 2018a [9] and for details of its precursor software see Ilyin 2000 [14]). Also, the use of predetermined observing blocks for one night is now implemented. It can also be executed in remote control.

6. FIRST SCIENCE

6.1 PEPSI "deep spectrum" project

As part of the first PEPSI key-science project, we aim to provide well-exposed and average-combined (*viz*. deep) high-resolution spectra of representative stellar targets. Such deep spectra contain an overwhelming amount of information, typically much more than what could be analyzed and discussed within a single publication. Therefore, these spectra are made available in form of (electronic) atlases and can be downloaded as FITS files from https://pepsi.aip.de. Such a deep spectrum may be viewed as an analog of the successful "Hubble Deep Field". The first star in this series of papers was our Sun (Strassmeier et al. 2018a [9]). It also acted as a system-performance cornerstone. So far, we observed approximately 50 targets (Strassmeier et al. 2018b [13]), among them as elusive objects as Kepler-444 (Mack et al. 2018 [15]) or bright famous benchmark objects like Arcturus, Procyon, and even Sirius (the brightest star in the sky with a 12m telescope!).

Two spectra of Boyajian's "Tabby's" star (KIC8462852) were obtained on June 1 and 2, 2017 (i.e., actually four spectra because the LBT is a binocular telescope). Both spectra were taken in medium-resolution mode with the 200-μm fiber enabling R=130,000 with 4.2-pix sampling. Three integrations per spectrum covered the entire optical and near-IR range from 384 to 913 nm. Total integration time was 70 minutes except for the last integration of the second exposure (60 min) due to sky brightness. S/N per pixel was up to 200 in the red and up to 150 in the blue. Figure 11 shows a 1.3-Å excerpt of the wavelength region around the Na D_1 line. Both D lines appear equally structured with two dominating line components, each one again made up of several more but unresolved sub-components. No difference was seen from one day to the other. It may indicate that the ominous brightness dips of KIC8462852 are related with circumstellar and/or interstellar material rather than of stellar or even extraterrestrial-civilization origin (*cf.* Boyajian et al. 2018 [16]).

Downloaded From: https://www.spiedigitallibrary.org/conference-proceedings-of-spie on 06 Dec 2019
Terms of Use: https://www.spiedigitallibrary.org/terms-of-use

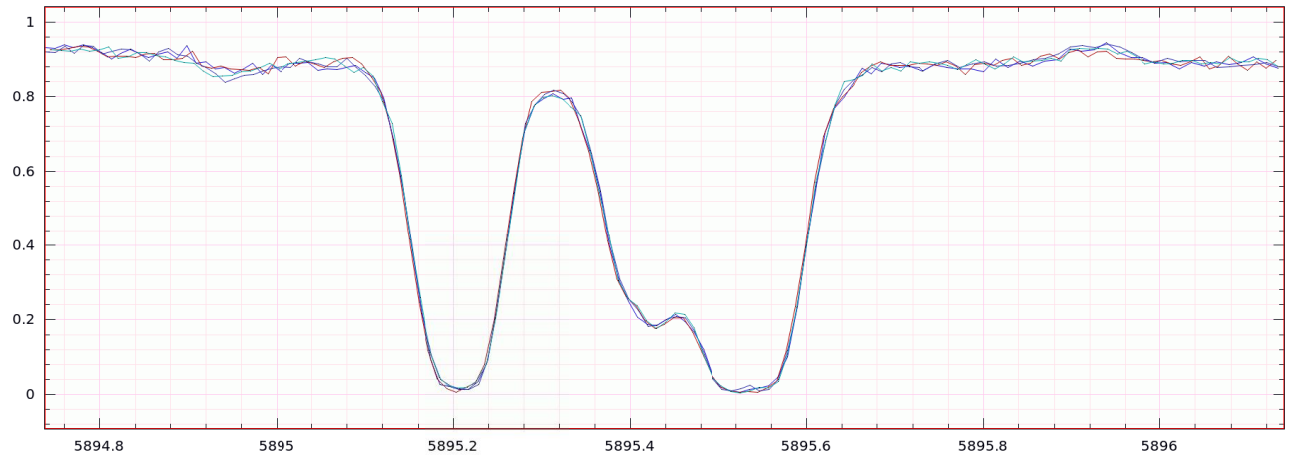

Figure 11. Close-up of the sodium D_1 line of Boyajian's star (KIC8462852, V=12.0 mag). The *y*-axis is normalized intensity, the *x*-axis wavelength in Ångströms. Four spectra are overplotted from two different nights. Spectral resolution is 130,000 with a sampling of 4.2 pixels per resolution element. S/N per pixel is 200. Integration time was 70 min under mediocre conditions. The spectra show three distinct line components, each one likely made up by several subcomponents, and appear to be of interstellar origin. Stellar lines are broadened by 80 km/s and are very shallow with a residual depth of around 0.9.

Another type of application aims towards revised abundances of the local interstellar medium (LISM). Due to its brightness and clean stellar spectrum, ζ Oph has been a standard background target for LISM work and is well searched for interstellar absorption lines including the very weak Li I ISM lines (Kawanomoto et al. 2009 [17], and references therein). A deep high-resolution spectrum of ζ Oph was obtained along with Tabby's star on June 1, 2017 (Fig. 12). Individual spectra were obtained with PEPSI in its $R \approx 250{,}000$ mode. The combined spectrum has a peak S/N of 1,800 per pixel around 700 nm with an S/N average of ≈1,300 across the full wavelength range. Integration time was 2×5 min.

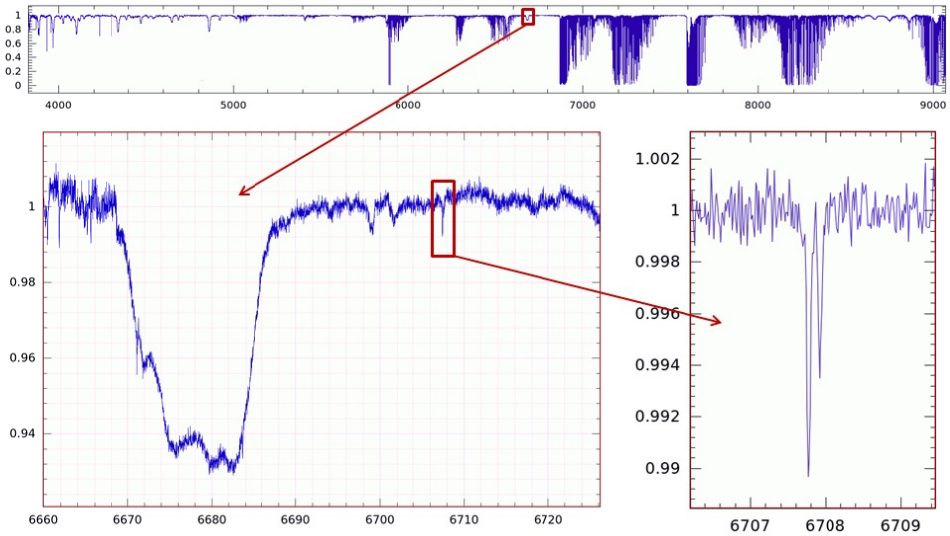

Figure 12. Deep PEPSI spectrum of ζ Oph (O9IV) and its LISM lines. The *x*-axes are wavelengths in Å, the *y*-axes relative intensity. *Top.* The full spectrum from 384-913 nm. Several strong ISM lines are seen in the blue part, the red part is dominated by telluric lines. *Bottom left.* Zoom into the stellar He I 6680 line (deformed by non-radial pulsations). *Bottom right.* The resolved Li doublet at 6708 Å from the LISM. Spectral resolution is ≈250,000, peak S/N is 1,800.

Downloaded From: https://www.spiedigitallibrary.org/conference-proceedings-of-spie on 06 Dec 2019
Terms of Use: https://www.spiedigitallibrary.org/terms-of-use

6.2 Exoplanet transits

When a planet transits a rotating star, the obscured regions of the stellar disk do not contribute to the formation of the rotationally-broadened stellar absorption line profile. The subtracted light results in a perturbation of the line profile at velocities corresponding to the radial velocities of the obscured surface elements. For sufficiently rapid rotation and/or sufficiently high spectral resolution, one can spectroscopically resolve the rotationally-broadened line profile and the line profile perturbation. This has been achieved for a transit of the hot Jupiter KELT-21b around the $V = 10.5$-mag A8V star HD 332124 (Fig. 13; Johnson et al. 2018 [18]).

Transit observations were carried out on 2017 May 29 and lasted for 4 continuous hours concluding when closing for sunrise. Integration time was set to 1,200 s. CCD read-out and overhead summed up to 90 s and enabled a sequence of 13 back-to-back spectra. The target altitude was very low at the beginning of the observing sequence with an air mass of 2.1. The sky was clear and seeing at the start of the sequence was 1.0″ but deteriorated to 1.3″ at the end of the sequence. Peak S/N was 140 and 100 per pixel in CD IV and CD II, respectively.

The analysis of these data by Johnson et al. (2018 [18]) demonstrated that the planetary orbit of KELT-21b is well-aligned with the stellar spin axis, with a sky-projected spin–orbit misalignment of just 6±2 degrees.

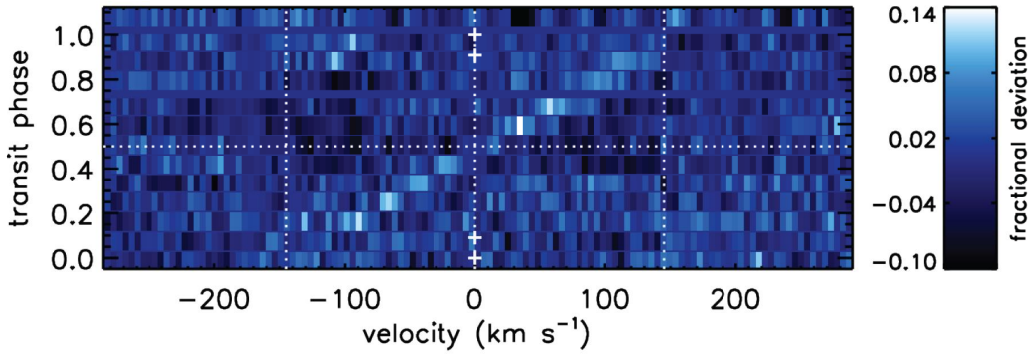

Figure 13. Residual line profiles for a transit of KELT-21b. Time increases from bottom to top, the color scale shows the deviation of the line profile from the average line profile. The transit is the bright streak moving from lower left to upper right. Vertical lines mark the center of the line profile at v = 0 and the edges at v = ± v sin i, a horizontal line shows the time of mid-transit, and the four small crosses depict the times of first through fourth contacts.

In another S/N league is the famous planet-host star TRAPPIST-1 with its seven terrestrial-size planets. With a V magnitude of 18.8 mag and an I magnitude of 14.0 mag (M8 spectral type) it is on the faint end of what PEPSI can do. One transit of planet g was followed in November 2017 in order to test the capability of PEPSI and possibly probe a Rossiter-McLaughlin effect (Fig. 14). Transit duration was one hour and ten minutes.

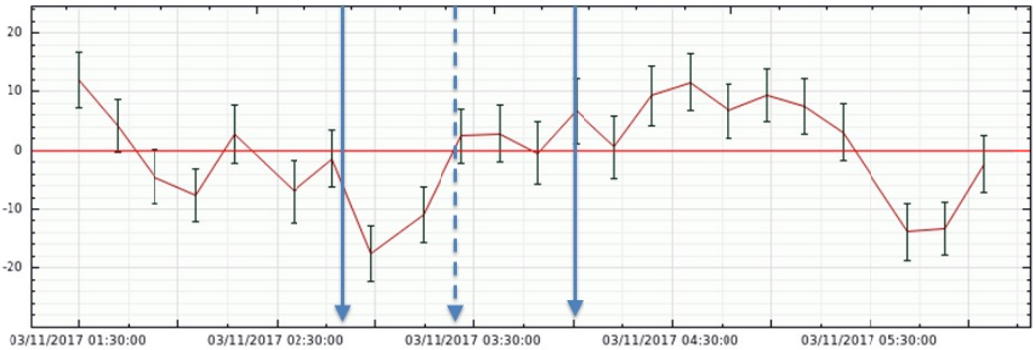

Figure 14. Preliminary residual radial velocities (in m/s) for a transit of TRAPPIST-1g on the night of Nov. 3, 2017. A trend was removed with a linear fit in order to search for a Rossiter-McLaughlin effect. Transit mid-point was at 03:26 UT (dashed arrow), transit start was at ≈02:50 UT, and end was at ≈04:00 UT (full-line arrows).

Downloaded From: https://www.spiedigitallibrary.org/conference-proceedings-of-spie on 06 Dec 2019
Terms of Use: https://www.spiedigitallibrary.org/terms-of-use

6.3 Stellar surfaces

Solar analogy thaught us that the surface spot distribution is a fingerprint of the underlying dynamo process and its subsequent magnetic-field eruption is seen in forms of sunspots or sunspot groups. On stars, we resolve the surface only by an indirect tomographic imaging technique, called Doppler imaging, and map the surface temperature or brightness distribution as a proxy of the magnetic field. This technique was introduced to cool stars close to 40 years ago (Vogt & Penrod 1983 [19], see also the review by Strassmeier 2009 [20]). It requires high-resolution spectra well sampled over a rotation period of the star but also a target star with rapid rotation so that the line broadening is dominated by Doppler broadening. We present the first Doppler image from PEPSI of the young solar analog EK Draconis (Fig. 15; Järvinen et al. 2018 [21]). It employed a spectral resolution of on average 230,000 (blue to red) that translates to approximately 25–30 resolution elements across the stellar disk of EK Dra. With this, an unprecedented surface resolution was achieved and possibly led to the discovery of a starspot with a penumbra, just like we see on the Sun in white light.

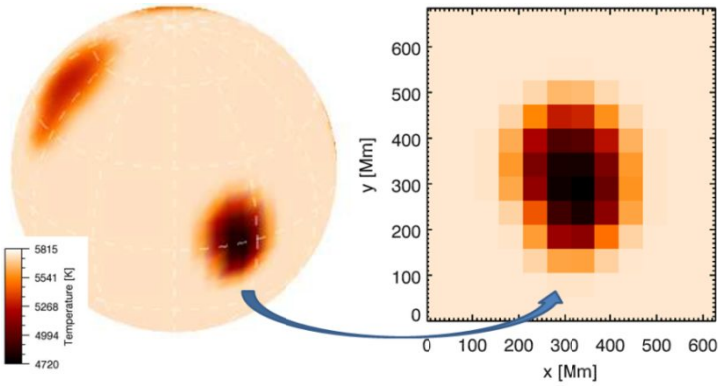

Figure 15. Doppler image of the surface of the G2 star EK Draconis. Bottom left is its temperature scale in Kelvin. The image to the right is a de-projected zoom into the one isolated equatorial starspot seen in the full image.

6.4 Novae

The classical nova V5668 Sgr was discovered on 2015 March 15. We obtained high resolution optical spectroscopy on 30 nights between 2015 April 3 and 2016 June 5 with the LBT and VATT. The spectra cover all or part of the 3835-9065 Å spectral region at a resolution of up to 250,000 (1.2 km/s). The early spectra are dominated by emission lines of the Balmer and Paschen series of hydrogen, Fe II, Ca II, and Na I with P Cyg-type line profiles as well as emission lines of [O I]. Numerous interstellar lines and bands are readily apparent at high spectral resolution. The permitted line profiles show complex and dramatic variations in the multi-component P Cyg-type line profiles with time. We detect a weak blue-shifted absorption line at a velocity consistent with Li I 6708 Å when compared with the line profiles of Hβ, Fe II 5169 Å, and Na I D (Wagner et al. 2018 [22]).

6.5 Polarimetry

The polarimeters were commissioned in October 2017 but no publications exist at the submission of the present paper. A well-exposed spectrum of the magnetic standard A9V star γ Equ showed a null spectrum with an rms of better than 10^{-3} for a selected wavelength range near 5480Å. It corresponds to an S/N of 1180 (see the spectrum in Fig. 5 in Sect. 2.6). Integration time was 12 min. This appears to be about a factor 2 ½ better than the corresponding null spectrum of the same star obtained with HARPS-Pol (Snik et al. 2013 [23]) in 24 min and is due to a combination of superior S/N as well as very low (not yet measurable) CP-LP cross talk.

ACKNOWLEDGEMENTS. We thank all engineers and technicians involved in PEPSI, in particular our Forschungstechnik team and its late head Emil Popow who passed away much too early. Special thanks are also due to former mountain manager John Little and his entire LBTO mountain crew and particularly to Mike Lesser and his University of Arizona ITL CCD aficionados without whom we could not have solved the zillions of problems. It is also a pleasure to thank the German Federal Ministry (BMBF) for the year-long support for the construction of PEPSI through their Verbundforschung grants 05AL2BA1/3 and 05A08BAC.

Downloaded From: https://www.spiedigitallibrary.org/conference-proceedings-of-spie on 06 Dec 2019
Terms of Use: https://www.spiedigitallibrary.org/terms-of-use

REFERENCES

[1] Strassmeier, K. G., Ilyin, I., Jaervinen, A., et al., "PEPSI: The high-resolution echelle spectrograph and polarimeter for the Large Binocular Telescope", AN 336, 324-361 (2015).

[2] Blanco-Cuaresma, S., Soubiran, C., Jofre, P., & Heiter, U., "The Gaia FGK benchmark stars. High resolution spectral library", A&A 566, A98 (2014).

[3] Mayor, M., Pepe, F., Queloz, D., et al., "Setting New Standards with HARPS", The Messenger 114, 20-24 (2003).

[4] Auriére, M., "Stellar Polarimetry with NARVAL", in EAS Publ. Ser. 9, eds. J. Arnaud & N. Meunier, p.105 (2003).

[5] Paletou, F., Böhm, T., Watson, V., & Trouilhet, J.-F., "Inversion of stellar fundamental parameters from ESPaDOnS and Narval high-resolution spectra", A&A, 573, A67 (2015).

[6] Dekker, H., D'Odorico, S., Kaufer, A., Delabre, B., & Kotzlowski, H., „Design, construction, and performance of UVES, the echelle spectrograph for the UT2 Kueyen Telescope at the ESO Paranal Observatory", SPIE, 4008, 534-545 (2000).

[7] Bagnulo, S., Jehin, E., Ledoux, C., et al., „The UVES Paranal Observatory Project: A Library of High-Resolution Spectra of Stars across the Hertzsprung-Russell Diagram", The Messenger, 114, 10-14 (2003).

[8] Dravins, D., "High-fidelity spectroscopy at the highest resolutions", AN 331, 535 (2010).

[9] Strassmeier, K. G.; Ilyin, I.; Steffen, M., „PEPSI deep spectra. I. The Sun-as-a-star", A&A 612, A44 (2018).

[10] Beckert, E., Strassmeier, K. G., Woche, M., Harnisch, G., Hornaff, M., Weber, M., Barnes, S., „Multi-resolution waveguide image slicer for the PEPSI instrument", SPIE 9912, 99125 (2016).

[11] Molaro, P., Esposito, M., Monai, S., et al., "A frequency comb calibrated solar atlas" A&A 560, A61 (2013).

[12] Bredthauer, G. & Boggs, K., "Status report on STA detectors and electronics for 2016", SPIE 9915, 99150 (2016).

[13] Strassmeier, K. G.; Ilyin, I.; Weber, M., „PEPSI deep spectra. II. Gaia benchmark stars and other M-K standards", A&A 612, A45 (2018).

[14] Ilyin, I., "High resolution SOFIN CCD echelle spectroscopy", PhD dissertation, Univ. of Oulu, Finland (2000).

[15] Mack, C. E., III; Strassmeier, K. G.; Ilyin, I.; Schuler, S. C.; Spada, F.; Barnes, S. A., "PEPSI deep spectra. III. A chemical analysis of the ancient planet-host star Kepler-444", A&A 612, A46 (2018).

[16] Boyajian, T. S., Alonso, R., Ammerman, A., et al., "The first post-Kepler brightness dips of KIC8462852", ApJ 853, L8 (2018).

[17] Kawanomoto, S. et al., "The New Detections of ^{7}Li/^{6}Li Isotopic Ratio in the Interstellar Media", ApJ 701, 1506 (2009).

[18] Johnson et al., "KELT-21b: A Hot Jupiter Transiting the Rapidly Rotating Metal-poor Late-A Primary of a Likely Hierarchical Triple System", AJ 155, 100 (2018).

[19] Vogt, S. S. & Penrod, G. D., "Doppler Imaging of spotted stars - Application to the RS Canum Venaticorum star HR 1099", PASP 95, 565 (1983).

[20] Strassmeier, K. G., "Starspots", A&ARv 17, 251 (2009).

[21] Järvinen, S., Strassmeier, K. G., Carroll, T., Ilyin, I., Weber, M., "Mapping EK Dra with PEPSI. "Evidence for starspot penumbrae", A&A, submitted (2018).

[22] Wagner, R. M., Woodward, C. E., Starrfield, S., Ilyin, I., Strassmeier, K.G., "High Resolution Optical Spectroscopy of the Classical Nova V5668 Sgr Showing the Presence of Lithium", AAS Meeting #231, id.#358.10 (2018).

[23] Snik, F. et al., "The polarimeters for HARPS and X-shooter", ASPC 470, 401 (2013).

Downloaded From: https://www.spiedigitallibrary.org/conference-proceedings-of-spie on 06 Dec 2019
Terms of Use: https://www.spiedigitallibrary.org/terms-of-use